A Novel Tensor Distribution Model for the Diffusion Weighted MR Signal

Baba C. Vemuri

UFRF Professor & Director
Center for Vision, Graphics, and Medical Imaging
Department of Computer & Information Science and Engineering
University of Florida

Joint work with Bing Jian, Evren Ozarslan, Paul Carney and Thomas Mareci

September 2006

Outline

Outline

Motivation

Diffusion Weighted MRI is an in vivo imaging modality that can be used to study connectivity patterns (e.g., in cognitive science) and changes in them due to pathology (e.g., Alzheimers Disease, Epilepsy etc)

Diagnosis of Injury and Disease

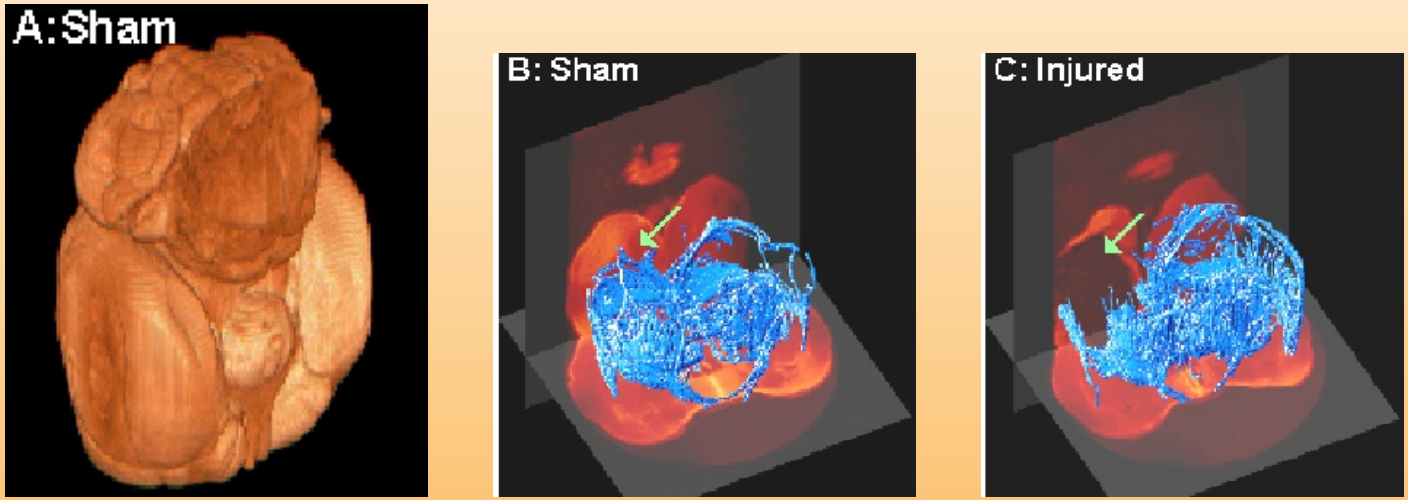

(a) (b) (c)

(a) Sham; (b) White matter fiber bundles in (a); (c) Injured brain.

Figure: Changes in connectivity due to injury

Outline

Diffusion Process

- Diffusion is driven by random molecular motion.
- Diffusion may be (isotropic) or (anisotropic)

Figure: Isotropic Diffusion

Diffusion Process

- Diffusion is driven by random molecular motion.
- Diffusion may be (isotropic) or (anisotropic)

Figure: Diffusion in structured medium.

Diffusion in Tissue

- Tissue can restrict molecular motion resulting in anisotropy.
- Can infer connectivity by analyzing diffusion properties.
- Disease and injury change diffusion properties.

Cf. Virtual Hospital (http://www.vh.org/)

Diffusion MRI

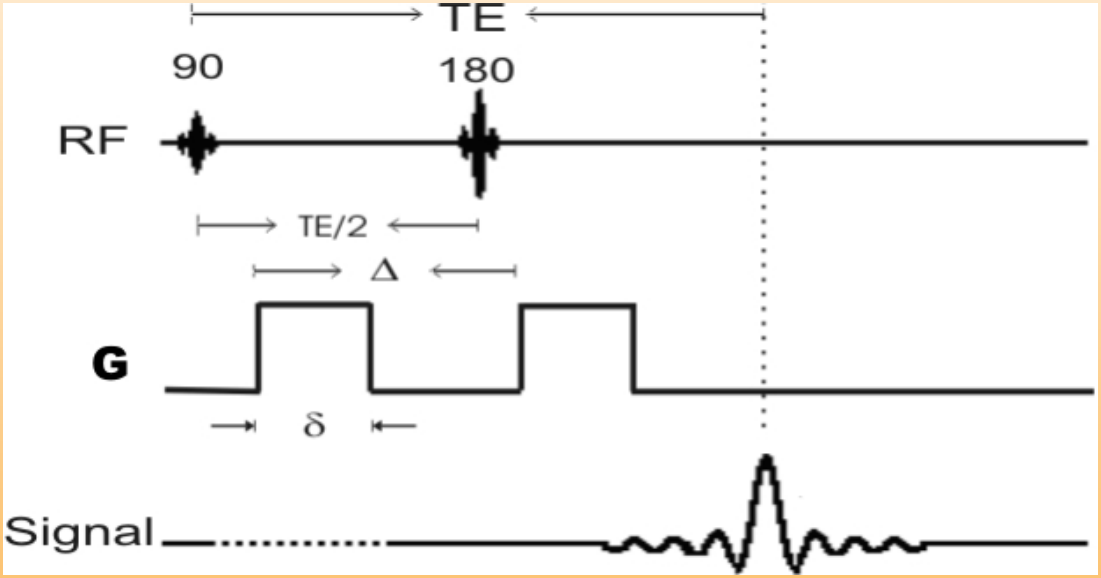

Diffusion gradients are introduced into a spin-echo pulse sequence. The signal attenuates according to the Stejskal-Tanner formula:

$$S = S_0 \exp\left(-\gamma^2 \delta^2 G^2 (\Delta - \delta/3) D\right)$$

γ : Gyromagnetic ratio
D : Apparent diffusion coefficient

Diffusion MRI (Contd.)

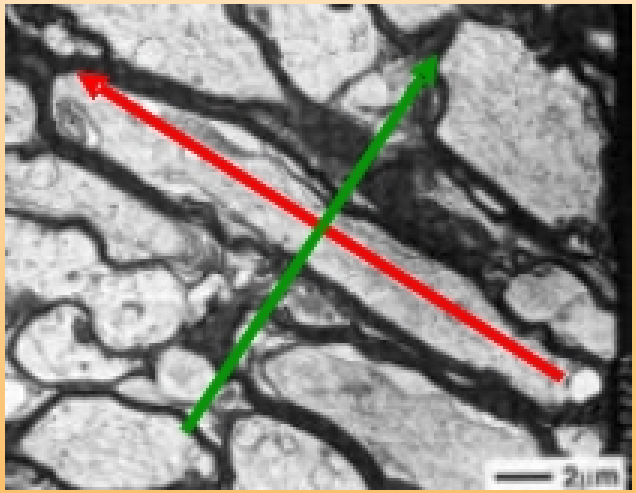

Stanisz et al. *Magn Reson Med* 1997:103-111.

The signal and the diffusion coefficients are orientation dependent.

Diffusion-Weighted Imaging

Stejskal-Tanner Equation

The relation between signal attenuation and diffusion coefficient was formulated in 1965

$$S = S_0 \exp(-bd)$$

- b is the diffusion weighting factor.
- d is the **apparent diffusion coefficient**.
- S_0 is the image with no diffusion weighting.

Diffusion Tensor Imaging

Stejskal-Tanner Equation

If we acquire multiple images, S, we may fit a tensor model to the data

$$S = S_0 \exp(-bg^T Dg) \tag{1}$$

- b is the diffusion weighting factor of **G**.
- g is the diffusion encoding gradient direction
- D is the **apparent diffusion tensor**.
- S_0 is the image with no diffusion weighting.

DT-MRI Contd.

- The diffusion tensor **D** is characterized by an SPD (symmetric positive definite) matrix.

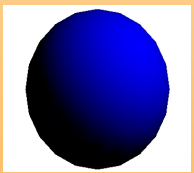

Isotropic Diffusion Tensor

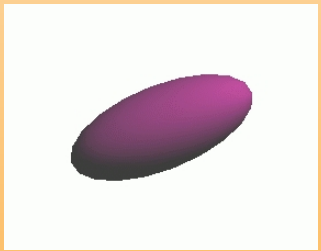

Anisotropic Diffusion Tensor

DTI Examples of Ellipsoid Visualization

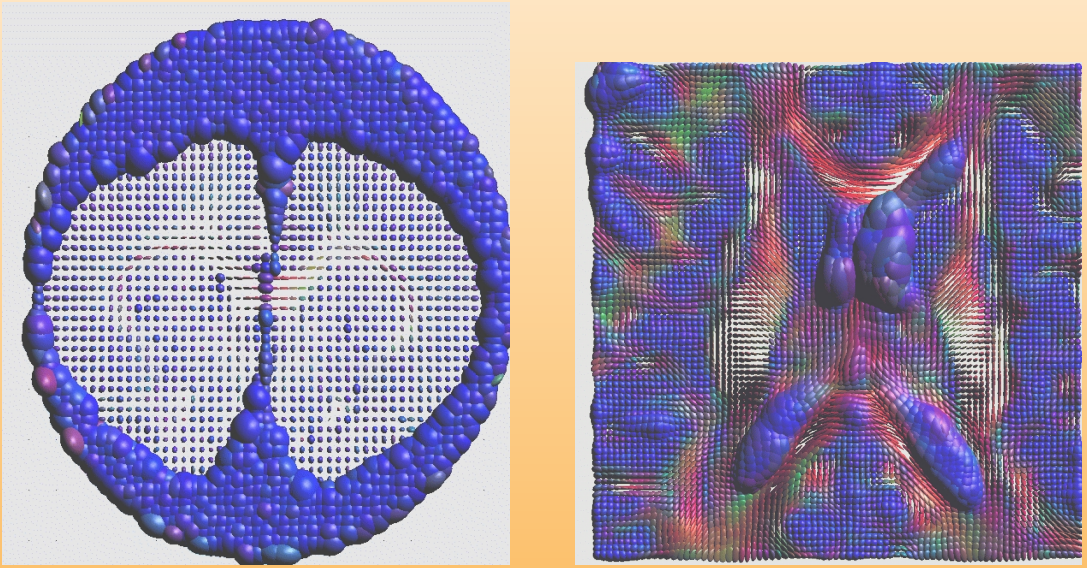

(a) Rat Brain (b) Human Brain

Figure: Ellipsoid Visualizations.

Fiber Tract Visualizations

- Ellipsoids, Stream lines, Stream tubes, LIC, Glyphs, Flouroscent particles and others (see Laidlaw Vis'98, Conturo et. al., PNAS'99, Parker ISMRM'00, IPMI'01, Vemuri et al., VLSM01, McGraw et al., MICCAI'02,MedIA'04, Chefd'Hotel et al., ECCV'02, Tschumperle ICCV'03, Zhang et al., TVCG'03 and many others)

Fiber Tract Mapping

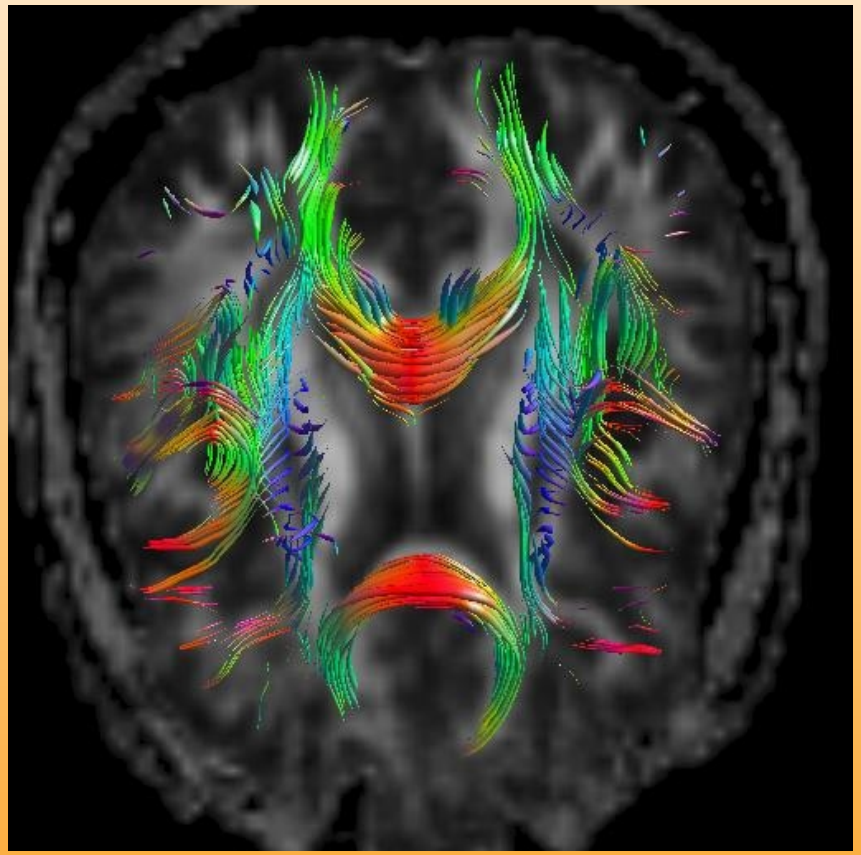

Stream tubes.

Fiber Tract Mapping from Restored DTI

Figure: Fiber tractography (stream tubes)

Fiber Tract Mapping (Contd.)

Figure: Fiber tractography (Lit particles)

Quantifying Anisotropy

Eigenvalue Decomposition of D

$$D = \begin{bmatrix} \mathbf{e_1}^T \\ \mathbf{e_2}^T \\ \mathbf{e_3}^T \end{bmatrix} \begin{bmatrix} \lambda_1 & 0 & 0 \\ 0 & \lambda_2 & 0 \\ 0 & 0 & \lambda_3 \end{bmatrix} \begin{bmatrix} \mathbf{e_1} & \mathbf{e_2} & \mathbf{e_3} \end{bmatrix}$$

Fractional Anisotropy

$$\mathrm{FA} = \sqrt{\frac{3}{2}} \sqrt{\frac{(\lambda_1 - \bar{\lambda})^2 + (\lambda_2 - \bar{\lambda})^2 + (\lambda_3 - \bar{\lambda})^2}{\lambda_1^2 + \lambda_2^2 + \lambda_3^2}}$$

- $\bar{\lambda} = \frac{1}{3}(\lambda_1 + \lambda_2 + \lambda_3)$
- For isotropic diffusion ($\lambda_1 = \lambda_2 = \lambda_3$) FA = 0
- For anisotropic diffusion ($\lambda_1 \gg \lambda_2 = \lambda_3$) FA $\rightarrow$ 1

Fractional Anisotropy

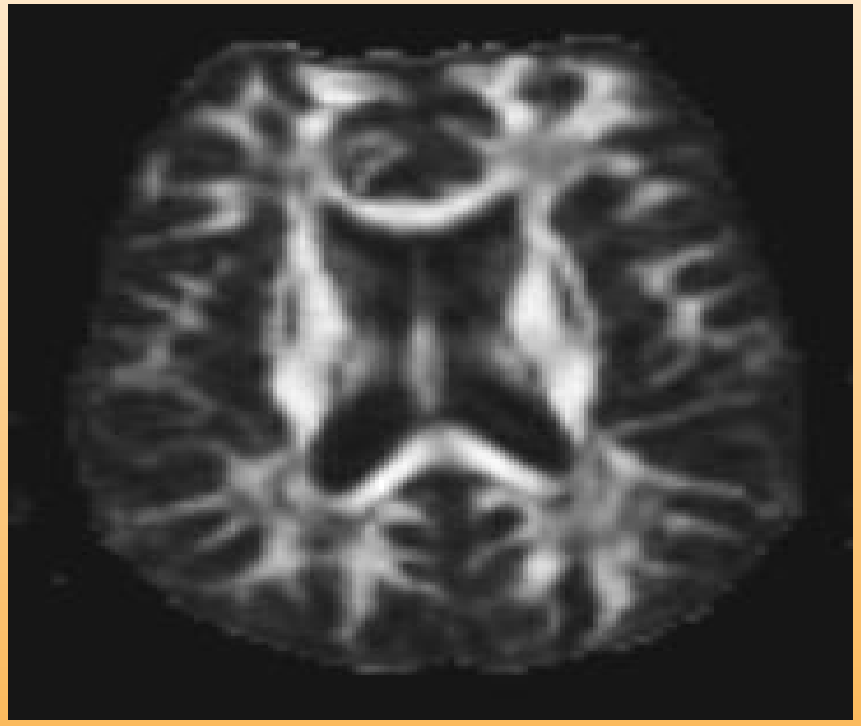

- Black: Water or cerebrospinal fluid (isotropic diffusion).
- White: White matter (highly anisotropic).
- Gray: Grey matter (less anisotropic).

DTI Segmentation

- Symmetrized KL (Wang & Vemuri CVPR'04, IEEE TMI'05)
- Riemanian Metric (Leglet et al., MICCAI'04, IPMI'05 and IEEE TMI'06)
- L2-metric (component-wise processing) – (Feddern et al., VLSM'03)
- Log-Euclidean Metric (Arsigny et. al., IPMI'05, MICCAI'05, IJCV'06, ISBI'06: applications to restoration, and registration. Segmentation, maybe coming soon?)

3D DTI Segmentation of the Corpus Callosum (Using KL-S)

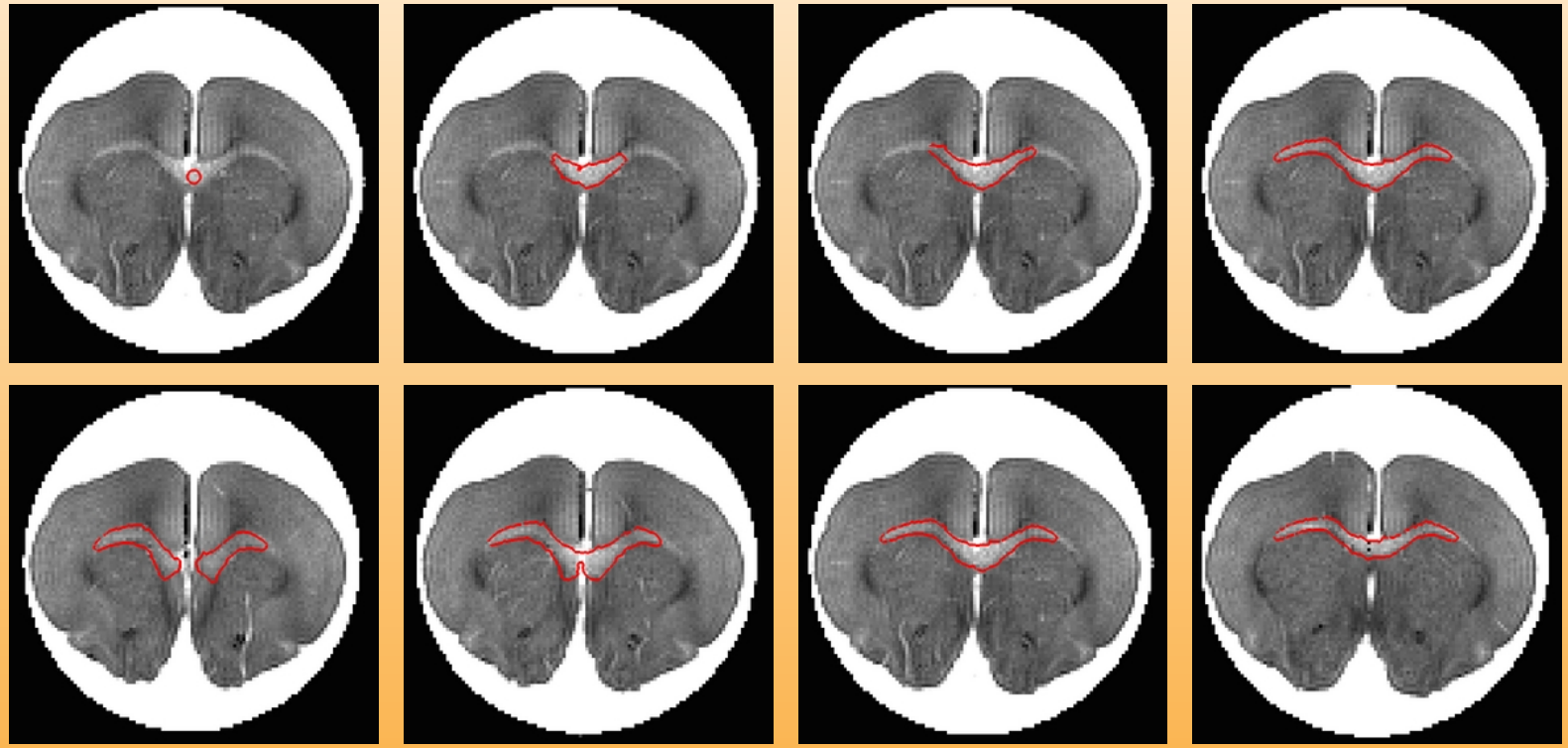

Figure: Top: a 2D slice of the corresponding evolving 3D segmentation superimposed on the D_{xx} component. Bottom: different 2D slices of the final segmentation superimposed on the D_{xx} component.

3D Segmented CC w/Mapped LIC

Figure: LIC Fiber Tracts on the CC

What is the Problem with DTI?

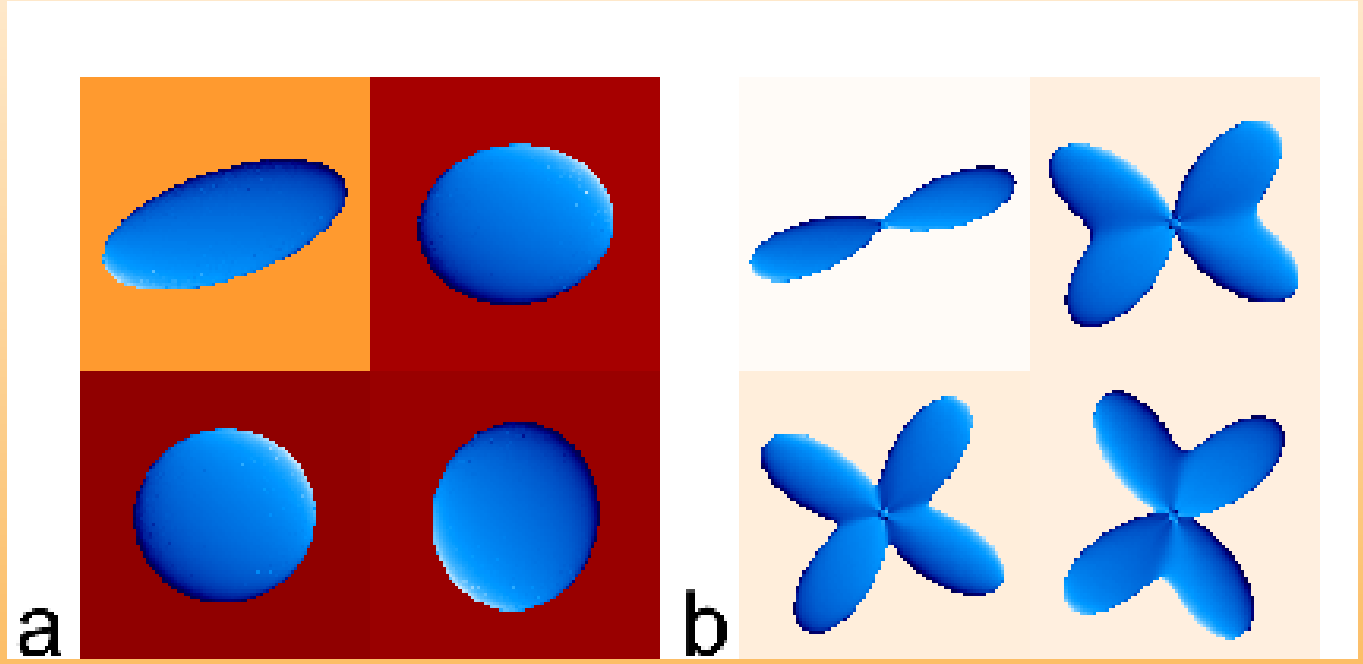

Figure: The effect of fiber orientation heterogeneity on diffusion MR measurements. (a) Iso-surfaces of the Gaussian probability maps assumed by DTI overlaid on FA maps computed from the DTs. (b) Probability profiles computed using the DOT from HARDI data overlaid on GA maps.

State of the Art

- HARDI: High-angular-resolution diffusion imaging. (Tuch et al. ISMRM'99)
- DSI: Diffusion spectrum imaging. (Wedeen et al. ISMRM'00)
- PAS: Persistent angular structure reconstruction. (Jasons and Alexander, IPMI'03)
- QBI: Q-ball imaging. (Tuch, MRM04)
- FORECAST: Fiber orientation estimated using continuous axially symmetric tensors (Anderson, MRM05)

State of the Art

- HARDI: High-angular-resolution diffusion imaging. (Tuch et al. ISMRM'99)
- DSI: Diffusion spectrum imaging. (Wedeen et al. ISMRM'00)
- PAS: Persistent angular structure reconstruction. (Jasons and Alexander, IPMI'03)
- QBI: Q-ball imaging. (Tuch, MRM04)
- FORECAST: Fiber orientation estimated using continuous axially symmetric tensors (Anderson, MRM05)

State of the Art

- HARDI: High-angular-resolution diffusion imaging. (Tuch et al. ISMRM'99)
- DSI: Diffusion spectrum imaging. (Wedeen et al. ISMRM'00)
- PAS: Persistent angular structure reconstruction. (Jasons and Alexander, IPMI'03)
- QBI: Q-ball imaging. (Tuch, MRM04)
- FORECAST: Fiber orientation estimated using continuous axially symmetric tensors (Anderson, MRM05)

State of the Art

- HARDI: High-angular-resolution diffusion imaging. (Tuch et al. ISMRM'99)
- DSI: Diffusion spectrum imaging. (Wedeen et al. ISMRM'00)
- PAS: Persistent angular structure reconstruction. (Jasons and Alexander, IPMI'03)
- QBI: Q-ball imaging. (Tuch, MRM04)
- FORECAST: Fiber orientation estimated using continuous axially symmetric tensors (Anderson, MRM05)

State of the Art

- HARDI: High-angular-resolution diffusion imaging. (Tuch et al. ISMRM'99)
- DSI: Diffusion spectrum imaging. (Wedeen et al. ISMRM'00)
- PAS: Persistent angular structure reconstruction. (Jasons and Alexander, IPMI'03)
- QBI: Q-ball imaging. (Tuch, MRM04)
- FORECAST: Fiber orientation estimated using continuous axially symmetric tensors (Anderson, MRM05)

Fundamental relationship

The MR signal measurement $S(\mathbf{q})$ and the average particle displacement density function $P(\mathbf{r})$ are related by the Fourier transform:

$$S(\mathbf{q}) = S_0 \int_{R^3} P(\mathbf{r})\, e^{j\mathbf{q}\cdot\mathbf{r}} d\mathbf{r}\ , \tag{2}$$

- S_0 : the signal in the absence of any diffusion gradient,
- $\mathbf{r}$: the displacement vector
- $\mathbf{q} = \gamma\delta G\mathbf{g}$,
  - γ is the gyromagnetic ratio,
  - δ is the diffusion gradient duration,
  - G and $\mathbf{g}$ are the magnitude and direction of the diffusion sensitizing gradients

The Diffusion tensor model

Assuming the oriented Gaussian model for $P(\mathbf{r})$ leads to the diffusion tensor model where the signal is expected to attenuate according to a Stejskal-Tanner like equation

$$S(\mathbf{q}) = S_0 \exp\left(-b\mathbf{g}^T \mathrm{D}\mathbf{g}\right), \tag{3}$$

where, $b = ||\mathbf{q}||^2 t$ is the b-factor, t is the effective diffusion time and $\mathbf{D}$ is the diffusion tensor.

Stejskal-Tanner equation and ADC profiles

More generally, for diffusion imaging studies use apparent diffusion coefficient (ADC) profiles which is governed by the Stejskal-Tanner equation:

$$S(\mathbf{q}) = S_0 exp(-bD_{app}) \tag{4}$$

where b : is the diffusion weighting factor depending on the strength as well as the effective time of the diffusion and D_{app} is the so called apparent diffusion coefficient.

Approaches using ADC Profiles

- Spherical harmonic expansion.
  - Frank MRM02
  - Alexander et al. MRM02
  - Chen et al. IPMI'05
- Generalized higher-order Cartesian tensors.
  - Ozarslan and Mareci, MRM03
  - Liu et al. MRM04
  - Descoteaux et al. SPIE'06

Approaches using ADC Profiles

- Spherical harmonic expansion.
  - Frank MRM02
  - Alexander et al. MRM02
  - Chen et al. IPMI'05
- Generalized higher-order Cartesian tensors.
  - Ozarslan and Mareci, MRM03
  - Liu et al. MRM04
  - Descoteaux et al. SPIE'06

Approaches using probability profiles

- Q-ball imaging: Funk-Radon transform. (Tuch MRM04)
- FORECAST (Anderson MRM05)
- MESD: Maximum Entropy Spherical Deconvolution (Alexander IPMI05),
- DOT: diffusion orientation transform. (Ozarslan et al. 2005)
- Hess et al. MRM06, Descoteaux et al. ISBI'06

Approaches using probability profiles

- Q-ball imaging: Funk-Radon transform. (Tuch MRM04)
- FORECAST (Anderson MRM05)
- MESD: Maximum Entropy Spherical Deconvolution (Alexander IPMI05),
- DOT: diffusion orientation transform. (Ozarslan et al. 2005)
- Hess et al. MRM06, Descoteaux et al. ISBI'06

Approaches using probability profiles

- Q-ball imaging: Funk-Radon transform. (Tuch MRM04)
- FORECAST (Anderson MRM05)
- MESD: Maximum Entropy Spherical Deconvolution (Alexander IPMI05),
- DOT: diffusion orientation transform. (Ozarslan et al. 2005)
- Hess et al. MRM06, Descoteaux et al. ISBI'06

Approaches using probability profiles

- Q-ball imaging: Funk-Radon transform. (Tuch MRM04)
- FORECAST (Anderson MRM05)
- MESD: Maximum Entropy Spherical Deconvolution (Alexander IPMI05),
- DOT: diffusion orientation transform. (Ozarslan et al. 2005)
- Hess et al. MRM06, Descoteaux et al. ISBI'06

Approaches using probability profiles

- Q-ball imaging: Funk-Radon transform. (Tuch MRM04)
- FORECAST (Anderson MRM05)
- MESD: Maximum Entropy Spherical Deconvolution (Alexander IPMI05),
- DOT: diffusion orientation transform. (Ozarslan et al. 2005)
- Hess et al. MRM06, Descoteaux et al. ISBI'06

Approaches using finite mixture model

- Tuch et al. 2002 assumes that the diffusion-attenuated MR signal is produced by a finite mixture of independent systems

$$S(\mathbf{q}) = S_0 \sum_j^n w_j \exp\left(-b\,\mathbf{g}^T \mathrm{D}_j \mathbf{g}\right),$$

where w_j is the apparent volume fraction of the compartment with diffusion tensor D_j.

- Related work: A. RamÃrez-Manzanares et al., VLSM'03and others.

Approaches using finite mixture model

- Tuch et al. 2002 assumes that the diffusion-attenuated MR signal is produced by a finite mixture of independent systems

$$S(\mathbf{q}) = S_0 \sum_j^n w_j \exp\left(-b\,\mathbf{g}^T \mathrm{D}_j \mathbf{g}\right),$$

  where w_j is the apparent volume fraction of the compartment with diffusion tensor D_j.
- Related work: A. RamÃrez-Manzanares et al., VLSM'03and others.

Proposed work: a novel statistical model

- Assume that at each voxel there is an underlying probability measure associated with $\mathcal{P}_n$, the manifold of $n \times n$ SPD matrices.
- An interesting observation: the resulting continuous mixture model and MR signal attenuation are related via a Laplace transform defined on $\mathcal{P}_n$.

Proposed work: a novel statistical model

- Assume that at each voxel there is an underlying probability measure associated with $\mathcal{P}_n$, the manifold of $n \times n$ SPD matrices.
- An interesting observation: the resulting continuous mixture model and MR signal attenuation are related via a Laplace transform defined on $\mathcal{P}_n$.

Proposed work: Highlights

- The Laplace transform can be evaluated in closed form for the case when the mixing distribution is a Wishart distribution.
- The resulting closed form gives a Rigaut-type function which has been used in the literature in the past to explain the MR signal decay but never with a rigorous mathematical derivation justifying it until now.
- Moreover, in this case, the traditional DTI model is the limiting case of the expected signal attenuation.

Proposed work: Highlights

- The Laplace transform can be evaluated in closed form for the case when the mixing distribution is a Wishart distribution.
- The resulting closed form gives a Rigaut-type function which has been used in the literature in the past to explain the MR signal decay but never with a rigorous mathematical derivation justifying it until now.
- Moreover, in this case, the traditional DTI model is the limiting case of the expected signal attenuation.

Proposed work: Highlights

- The Laplace transform can be evaluated in closed form for the case when the mixing distribution is a Wishart distribution.
- The resulting closed form gives a Rigaut-type function which has been used in the literature in the past to explain the MR signal decay but never with a rigorous mathematical derivation justifying it until now.
- Moreover, in this case, the traditional DTI model is the limiting case of the expected signal attenuation.

Proposed work: Applications

Current work:

- Leads to a new formula for diffusion tensor estimation
- Multi-fiber reconstruction using deconvolution technique

Proposed work: Applications

Current work:

- Leads to a new formula for diffusion tensor estimation
- Multi-fiber reconstruction using deconvolution technique

Our formulation

Let F be the underlying probability measure, then we can model the diffusion signal by:

$$\begin{aligned} S(\mathbf{q}) &= S_0 \int_{\mathcal{P}_n} \exp[-t\mathbf{q}^T \mathrm{D}\mathbf{q}]\, \mathrm{d}F(\mathrm{D}) \\ &= S_0 \int_{\mathcal{P}_n} f(\mathrm{D})\, \exp[-t\mathbf{q}^T \mathrm{D}\mathbf{q}]\, \mathrm{d}\mathrm{D} \end{aligned} \tag{5}$$

where $f(\mathrm{D})$ is the density function of F with respect to some carrier measure $\mathrm{d}\mathrm{D}$ on $\mathcal{P}_n$.

- $f(\mathrm{D})$: the density function of F with respect to some carrier measure $\mathrm{d}\mathrm{D}$ on $\mathcal{P}_n$.
- A more general form of mixture model with $f(\mathrm{D})$ being mixing density over the variance of Gaussians.
- Simplifies to the DTI model when the underlying probability

The Laplace transform on $\mathcal{P}_n$

Definition

The *Laplace transform* of $f : \mathcal{P}_n \to \mathbb{C}$, denoted by $\mathscr{L} f$, at the symmetric matrix $\mathrm{Z} \in \mathbb{C}^{n \times n}$ is defined by

$$\mathscr{L} f(\mathrm{Z}) = \int_{\mathcal{P}_n} f(\mathrm{Y}) \exp\left[-\mathrm{trace}(\mathrm{YZ})\right] \mathrm{dY} \,, \tag{6}$$

where $\mathrm{dY} = \prod \mathrm{d}y_{ij} \quad 1 \leq i \leq j \leq n$.

Above equation also defines the Laplace transform of the probability measure F on $\mathcal{P}_n$, which is denoted by $\mathscr{L} F$, when $\mathrm{d}F(\mathrm{Y}) = f(\mathrm{Y})\mathrm{dY}$.

The Statistical model

- Fact: $b\,\mathbf{g}^T \mathrm{D}\mathbf{g} = \mathrm{trace}(\mathrm{BD})$ where $\mathrm{B} = b\,\mathbf{g}\mathbf{g}^T$
- Observation: The diffusion signal model presented in the form of (5) can be exactly expressed as the Laplace transform of the probability measure F on $\mathcal{P}_n$, i.e. $S(\mathbf{q})/S_0 = (\mathscr{L}F)(\mathrm{B})$.
- The Statistical model:

$$S(\mathbf{q}) = S_0 \int_{\mathcal{P}_n} \exp\left(-\mathbf{q}^T \mathrm{D}\mathbf{q}\right) \mathrm{d}F(\mathrm{D}) = S_0(\mathscr{L}(F))(\mathrm{B}) \,, \quad (7)$$

where $\mathrm{B} = b\,\mathbf{g}\,\mathbf{g}^T$ and $\mathbf{g} = \mathbf{q}/|\mathbf{q}|$ as before.

Inverse problem

- Goal: recover a distribution $F(\mathrm{D})$ defined on $\mathcal{P}_n$ that best explains the observed diffusion signal $S(\mathbf{q})$.
- An ill-posed problem and in general not solvable without further assumptions.
- Proposed approach: assume that $F(\mathrm{D})$ belongs to some parametric probability family on $\mathcal{P}_n$, then estimate the parameters

Inverse problem

- Goal: recover a distribution $F(\mathrm{D})$ defined on $\mathcal{P}_n$ that best explains the observed diffusion signal $S(\mathbf{q})$.
- An ill-posed problem and in general not solvable without further assumptions.
- Proposed approach: assume that $F(\mathrm{D})$ belongs to some parametric probability family on $\mathcal{P}_n$, then estimate the parameters

Inverse problem

- Goal: recover a distribution $F(\mathrm{D})$ defined on $\mathcal{P}_n$ that best explains the observed diffusion signal $S(\mathbf{q})$.
- An ill-posed problem and in general not solvable without further assumptions.
- Proposed approach: assume that $F(\mathrm{D})$ belongs to some parametric probability family on $\mathcal{P}_n$, then estimate the parameters

Wishart distribution

Definition

(Letac and Massam, 1998)
For $\sigma \in \mathcal{P}_n$ and for p in $\Lambda = \left\{\frac{1}{2}, 1, \frac{3}{2}, \ldots, \frac{n-1}{2}\right\} \cup \left(\frac{n-1}{2}, \infty\right)$, the Wishart distribution $\gamma_{p,\sigma}$ with scale parameter σ and shape parameter p is defined as

$$\mathrm{d}\gamma_{p,\sigma}(\mathrm{Y}) = \Gamma_n(p)^{-1} \, |\mathrm{Y}|^{p-(n+1)/2} \, |\sigma|^{-p} \, \exp(-\mathrm{trace}(\sigma^{-1}\mathrm{Y})) \, \mathrm{dY}, \tag{8}$$

where Γ_n denotes the multivariate gamma function $\int_{\mathcal{P}_n} \exp\left(-\mathrm{trace}(\mathrm{Y})\right) \, |\mathrm{Y}|^{p-(n+1)/2} \, \mathrm{dY}$ and $|\cdot|$ denotes the determinant of a matrix.

A natural generalization of the gamma distribution

Remark

The expected value of a random variable(matrix) with a $\gamma_{p,\sigma}$ distribution is $p\sigma$.

Remark

The Laplace transform of the Wishart distribution $\gamma_{p,\sigma}$ is

$$\int \exp(-\mathrm{trace}(\theta u))\,\gamma_{p,\sigma}(\mathrm{d}u) = |I_n + \theta\sigma|^{-p} \quad \textit{where } (\theta + \sigma^{-1}) \in \mathcal{P}_n$$

Invariant measure

- The expected value $p\sigma$ does not correspond to the maximum value of the density function defined with respect to the Lebesgue measure induced from the space of symmetric matrices..
- $\mathcal{P}_n$ is a homogenous space under the action of the general linear group and has a $GL(n)-$invariant measure [Terras,1985] defined by $d\mu(Y) = |Y|^{-(n+1)/2} dY$.
- The density function w.r.t the above invariant measure is:

$$\begin{aligned} d\gamma_{p,\sigma}(Y) &= \Gamma_n(p)^{-1} |Y|^p |\sigma|^{-p} \exp(-\text{trace}(\sigma^{-1} Y))\, d\mu \\ &= \frac{|\sigma^{-1} Y|^p}{\Gamma_n(p)\, |\exp(\sigma^{-1} Y)|}\, d\mu, \end{aligned} \tag{9}$$

And it can be shown that this function does reach its maximum at the expected point $p\sigma$.

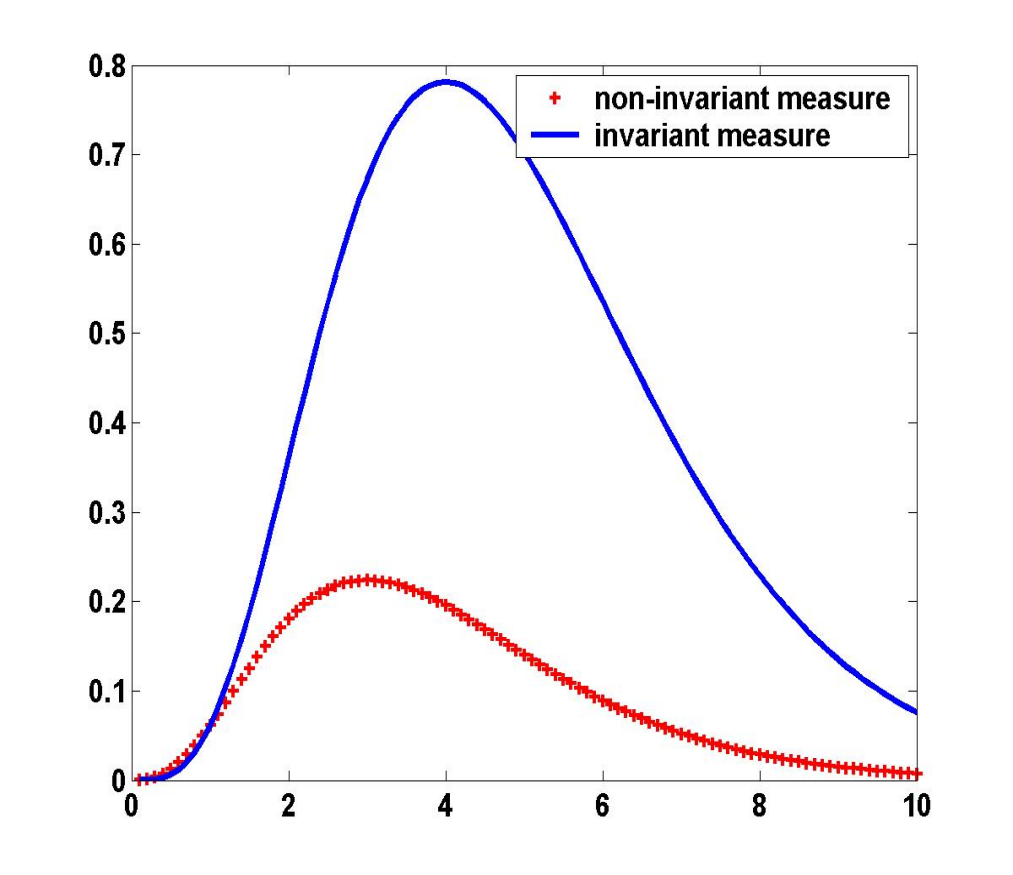

Figure: Plots of density functions of gamma distribution $\gamma_{4,1}$ w.r.t the non-invariant and scale-invariant measures respec. Note that the expected value 4 corresponds to the peak of the density function w.r.t. invariant measure but not for the non-invariant measure.

The Wishart distributed tensor model for DW-MRI

By substituting the general probability measure F with the Wishart measure $\gamma_{p,\sigma}$ and noting that $\mathrm{B} = b\,\mathbf{g}\,\mathbf{g}^T$, we have

$$\frac{S(\mathbf{q})}{S_0} = (\mathscr{L}\gamma_{p,\sigma})(\mathrm{B}) = |I_n + \mathrm{B}\sigma|^{-p} = (1 + (b\,\mathbf{g}^T\sigma\mathbf{g}))^{-p}\,. \quad (10)$$

Salient properties of the Wishart distributed tensor model

- Leads to a rigorous derivation of the Rigaut-type expression used to explain the MR signal behavior as a function of b.
- Mono-exponential model can be viewed as a limiting case when p tends to infinity.

Salient properties of the Wishart distributed tensor model

- Leads to a rigorous derivation of the Rigaut-type expression used to explain the MR signal behavior as a function of b.
- Mono-exponential model can be viewed as a limiting case when p tends to infinity.

Rigaut-type asymptotic fractal expression

Consider the family of Wishart distributions $\gamma_{p,\sigma}$ with fixed expected value $\hat{\mathrm{D}} = p\sigma$. In this case, the above expression takes the form:

$$S(\mathbf{q}) = S_0 \left(1 + (b\,\mathbf{g}^T \hat{\mathrm{D}} \mathbf{g})/p\right)^{-p}.$$

This familiar Rigaut-type asymptotic fractal expression implies a signal decay characterized by a power law in the large-b region which is the expected asymptotic behavior for the MR signal attenuation in porous media.

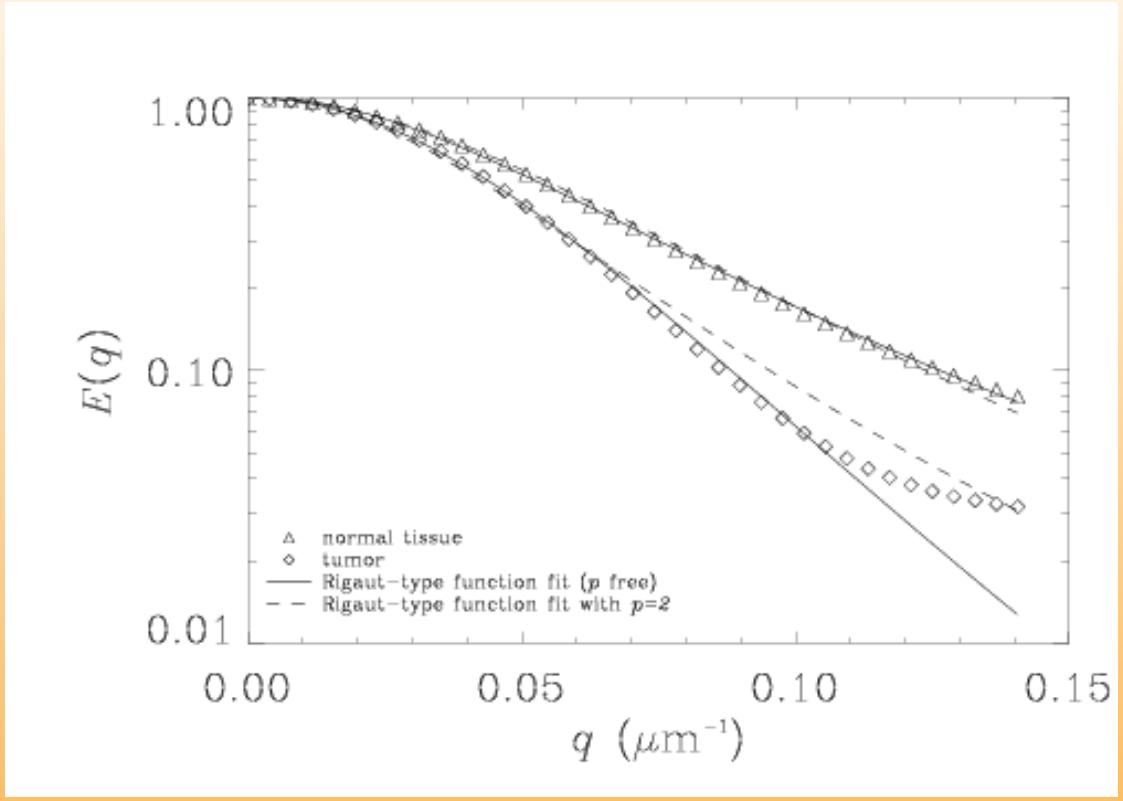

Figure: Plots of very high signal-to-noise-ratio spectroscopy data obtained from excised neural tissue samples.

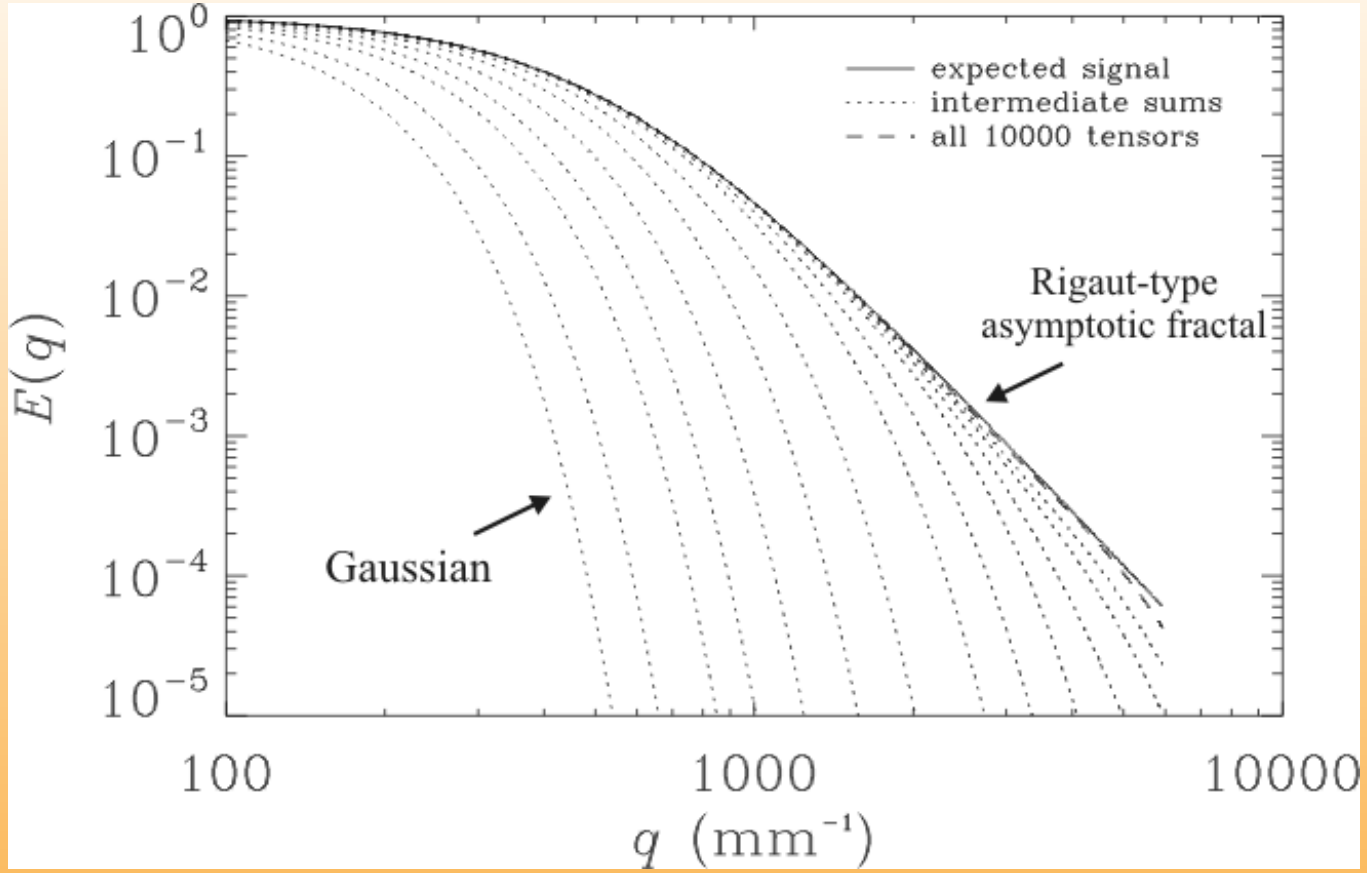

Figure: Plots illustrating the Wishart distributed tensors lead to a Rigaut-type signal decay.

Mono-exponential model as a limiting case

Note further that when $p \longrightarrow \infty$, we have

$$\begin{aligned} S(\mathbf{q}) &= S_0 \left(1 + (b\,\mathbf{g}^T \hat{\mathrm{D}} \mathbf{g})/p\right)^{-p} \\ &\longrightarrow S_0 \, \exp(-b\mathbf{g}^T \hat{\mathrm{D}} \mathbf{g}) \, , \end{aligned} \tag{11}$$

which implies that the mono-exponential model can be viewed as a limiting case of our model.

New framework for DT estimation

Consider a set of diffusion measurements performed in a voxel containing a single fiber bundle and use the Wishart distribution $\gamma_{p,\sigma}$ as the mixing distribution in eqn. (7), we obtain $\left(\frac{S_0}{S(\mathbf{q})}\right)^{1/p} - \text{trace}(\mathrm{B}\sigma) = 1$, or in the matrix form:

$$\begin{pmatrix} (S_1)^{-\frac{1}{p}} & B_{xx} & \cdots & 2B_{xz} \\ (S_2)^{-\frac{1}{p}} & B_{xx} & \cdots & 2B_{xz} \\ \cdots & \cdots & \cdots & \cdots \\ (S_K)^{-\frac{1}{p}} & B_{xx} & \cdots & 2B_{xz} \end{pmatrix} \begin{pmatrix} (S_0)^{\frac{1}{p}} \\ \sigma_{xx} \\ \cdots \\ \sigma_{xz} \end{pmatrix} = \begin{pmatrix} 1 \\ 1 \\ \cdots \\ 1 \end{pmatrix}, \quad (12)$$

where K is the number of measurements at each voxel and B_{ij} and σ_{ij} are the six components of the matrices B and σ, respectively.

Multi-fiber reconstruction

- Motivation:
  - The single Wishart model can not resolve the IVOH due to the single diffusion maximum per voxel.
- Method:
  - Use a discrete mixture of Wishart distribution model where the mixing distribution in eqn. (7) is expressed as a weighted sum of Wishart distributions, $\mathrm{d}F = \sum_{i=1}^{N} w_i \mathrm{d}\gamma_{p_i,\sigma_i}$.
  - Deconvolution technique

Multi-fiber reconstruction

- Motivation:
  - The single Wishart model can not resolve the IVOH due to the single diffusion maximum per voxel.
- Method:
  - Use a discrete mixture of Wishart distribution model where the mixing distribution in eqn. (7) is expressed as a weighted sum of Wishart distributions, $\mathrm{d}F = \sum_{i=1}^{N} w_i \mathrm{d}\gamma_{p_i,\sigma_i}$.
  - Deconvolution technique

Deconvolution technique

- Model: Mixture of Wisharts

$$dF = \sum_{i=1}^{N} w_i d\gamma_{p_i,\sigma_i}$$

- Assumptions:
  - All the p_i take the same value p
  - Fix the eigenvalues of σ_i to specified values $(\lambda_1, \lambda_2, \lambda_3) = \frac{1}{p}(1.5, 0.4, 0.4)\mu^2/ms$ according to physiological considerations. (C.f. Tuch's thesis 2002)
  - N unit vectors evenly distributed on the unit sphere are chosen as the principal directions of σ_i.

Deconvolution technique

- Model: Mixture of Wisharts

$$dF = \sum_{i=1}^{N} w_i d\gamma_{p_i,\sigma_i}$$

- Assumptions:
  - All the p_i take the same value p
  - Fix the eigenvalues of σ_i to specified values $(\lambda_1, \lambda_2, \lambda_3) = \frac{1}{p}(1.5, 0.4, 0.4)\mu^2/ms$ according to physiological considerations. (C.f. Tuch's thesis 2002)
  - N unit vectors evenly distributed on the unit sphere are chosen as the principal directions of σ_i.

Linear system again!

Equation:

$$S(\mathbf{q}) = S_0 \sum_{i=1}^{N} w_i (1 + \text{trace}(\mathrm{B}\sigma_i))^{-p} \tag{13}$$

For a set of measurements with wave number $\mathbf{q}_j$, $j = 1, \ldots, K$, formulate a linear system

$$\mathrm{A}\mathbf{w} = \mathbf{s},$$

where $\mathbf{s} = (S(\mathbf{q}_j)/S_0)$ is the vector of normalized measurements, $\mathbf{w} = (w_i)$, is the vector of basis function weights and A is the matrix with ji-th entry

$$A_{ji} = (1 + \text{trace}(\mathrm{B}_j\sigma_i))^{-p}.$$

Fiber orientations: Diffusivity or Probability?

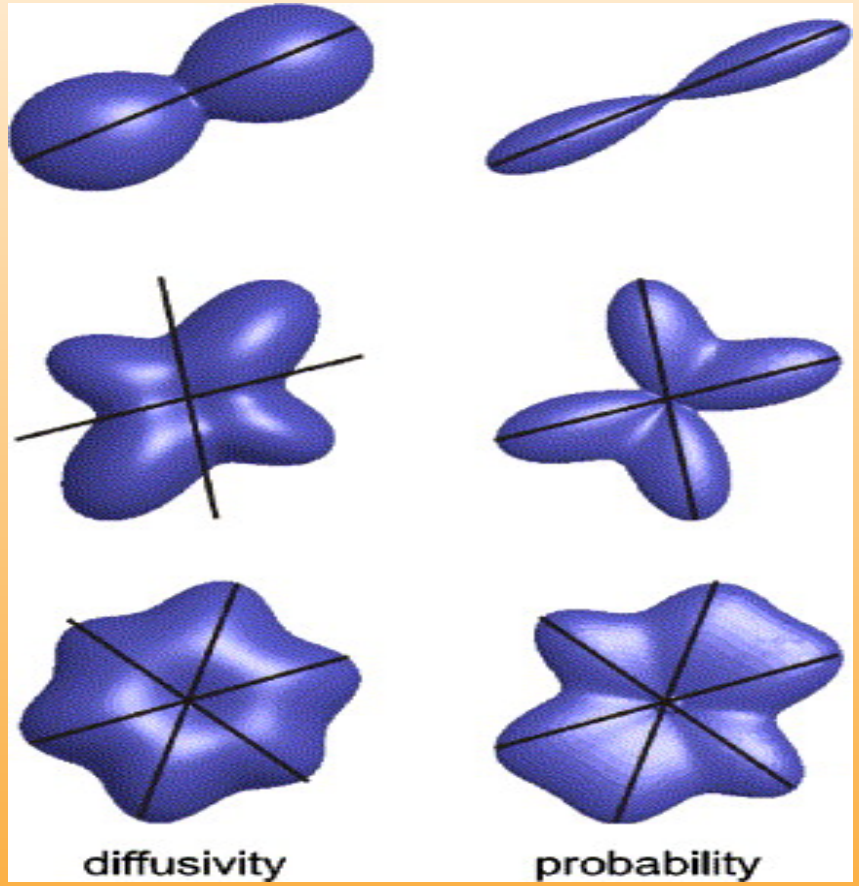

Figure: Diffusivity profile do not necessarily yield the orientations of the distinct fiber orientations. (Ozarslan et al. 2005) .

Fiber orientations: Diffusivity or Probability?

- To resolve fiber orientations, one need to find the peaks of the displacement probability surfaces.
- Recall the Fourier transform relationship:

$$P(\mathbf{r}) = \int E(\mathbf{q}) \exp(-i\mathbf{q} \cdot \mathbf{r})\, d\mathbf{q}$$

where $E(\mathbf{q}) = S(\mathbf{q})/S_0$ is the MR signal attenuation.

Fiber orientations: Diffusivity or Probability?

- To resolve fiber orientations, one need to find the peaks of the displacement probability surfaces.
- Recall the Fourier transform relationship:

$$P(\mathbf{r}) = \int E(\mathbf{q}) \exp(-i\mathbf{q} \cdot \mathbf{r})\, d\mathbf{q}$$

where $E(\mathbf{q}) = S(\mathbf{q})/S_0$ is the MR signal attenuation.

Our approach for resolving fiber orientations

- Assuming a continuous diffusion tensor model with mixing distribution $F(\mathrm{D}) = \sum_{i=1}^{N} w_i d\gamma_{p_i,\sigma_i}$, we get

$$\begin{aligned} P(\mathbf{r}) &= \int_{R^3} \int_{\mathcal{P}_n} \exp(-\mathbf{q}^T \mathrm{D}\mathbf{q}t)\, \mathrm{d}F(\mathrm{D})\, \exp(-i\mathbf{q}\cdot\mathbf{r})\, \mathrm{d}\mathbf{q} \\ &\approx \sum_{i=1}^{N} \frac{w_i}{\sqrt{(4\pi t)^3 |\hat{\mathrm{D}}_i|}} \exp(-\mathbf{r}^T \hat{\mathrm{D}}_i{}^{-1} \mathbf{r}/4t) \end{aligned} \tag{14}$$

where $\hat{\mathrm{D}}_i = p\sigma_i$ are the expected values of γ_{p,σ_i}.

Outline

Simulated data

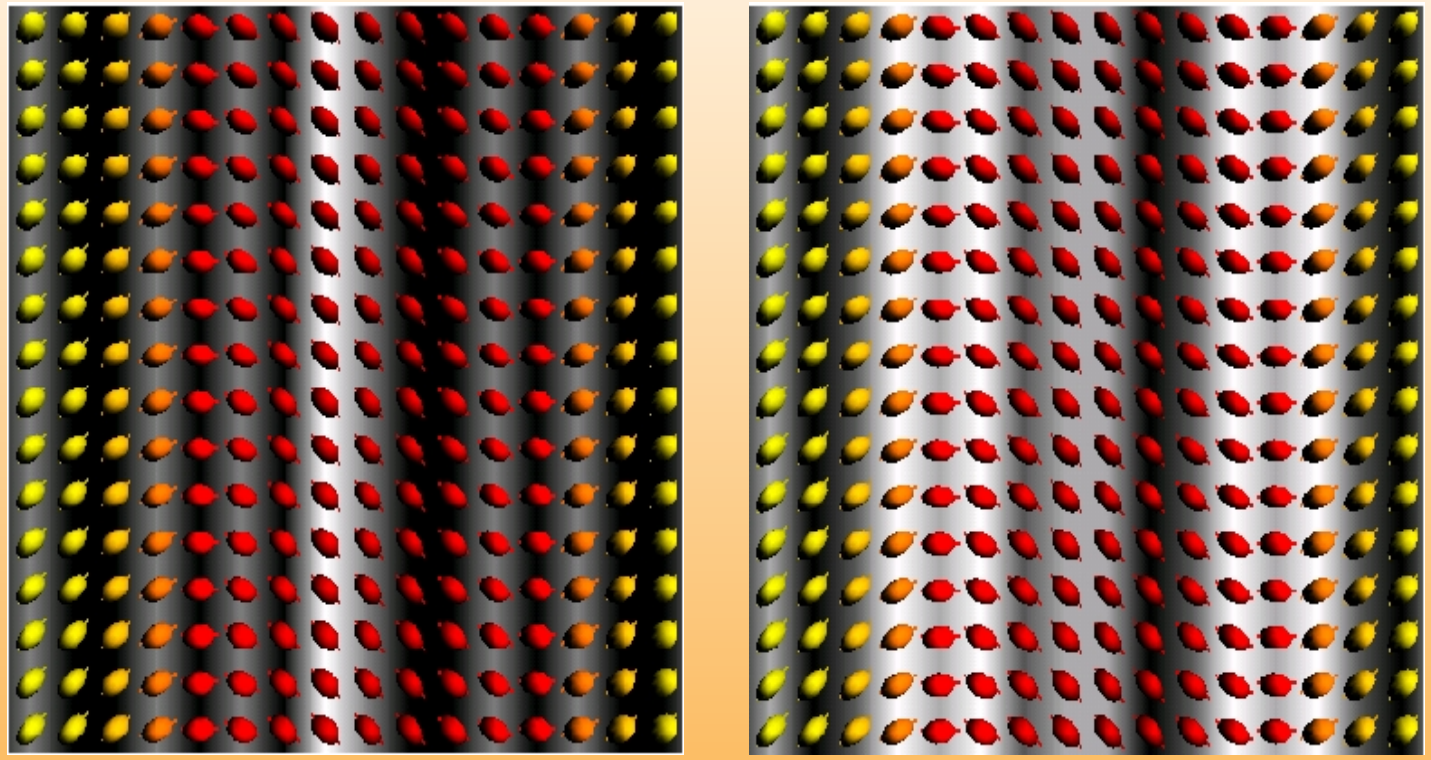

Figure: A synthetic data set representing single-fiber diffusion with sinusoidally varying orientations. Left: the tensor field obtained from fitting the linearized Stejskal-Tanner equation; Right: the tensor field using the Wishart model with $p = 2$.) .

	DTI model		Our model	
SNR	mean	std. dev.	mean	std. dev.
No noise	11.25	7.29	11.25	7.08
25*dB*	11.70	7.63	11.60	7.52
20*dB*	14.44	8.27	14.00	7.85
15*dB*	15.00	8.92	14.62	8.42

Table: Comparison of the accuracy of the estimated dominant eigenvectors using different methods under different noise levels.

Outline

Probability surfaces from simulated data

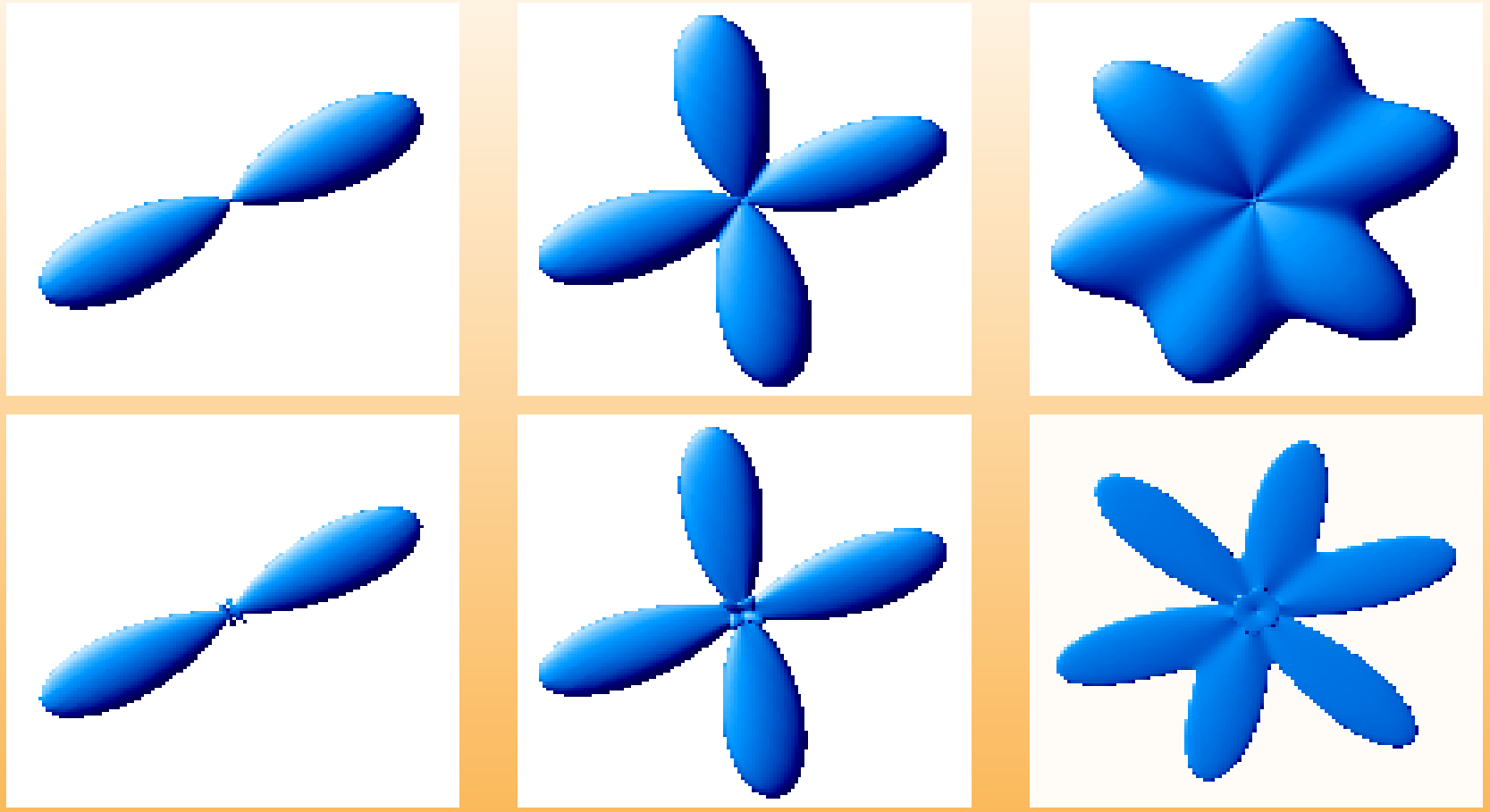

Figure: Simulations of 1-, 2- and 3-fibers ($b = 1500 s/mm^2$). Orientations: azimuthal angles $\phi_1 = 30, \phi_2 = \{20, 100\}, \phi_3 = \{20, 75, 135\}$; polar angles were all 90°. Top: Q-ball ODF surfaces computed using formula in (Anderson'05); Bottom: Probability surfaces computed using proposed method.

Resistance to noise (2-fibers, $\sigma = 0.08$)

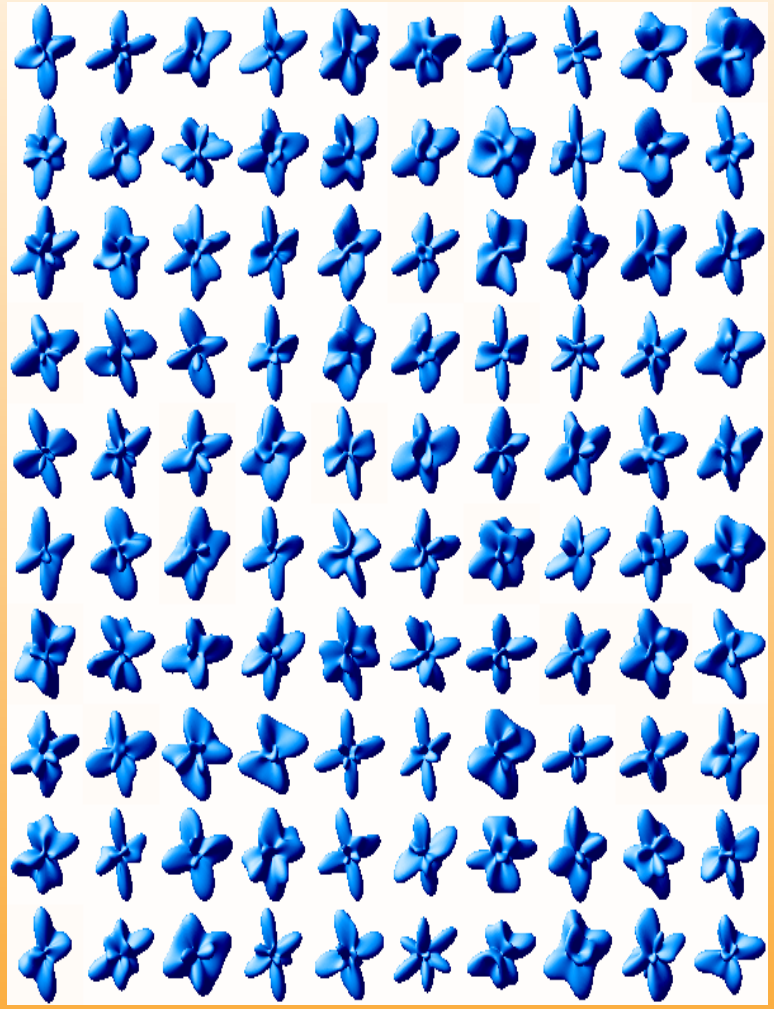

(a) ODF from QBI

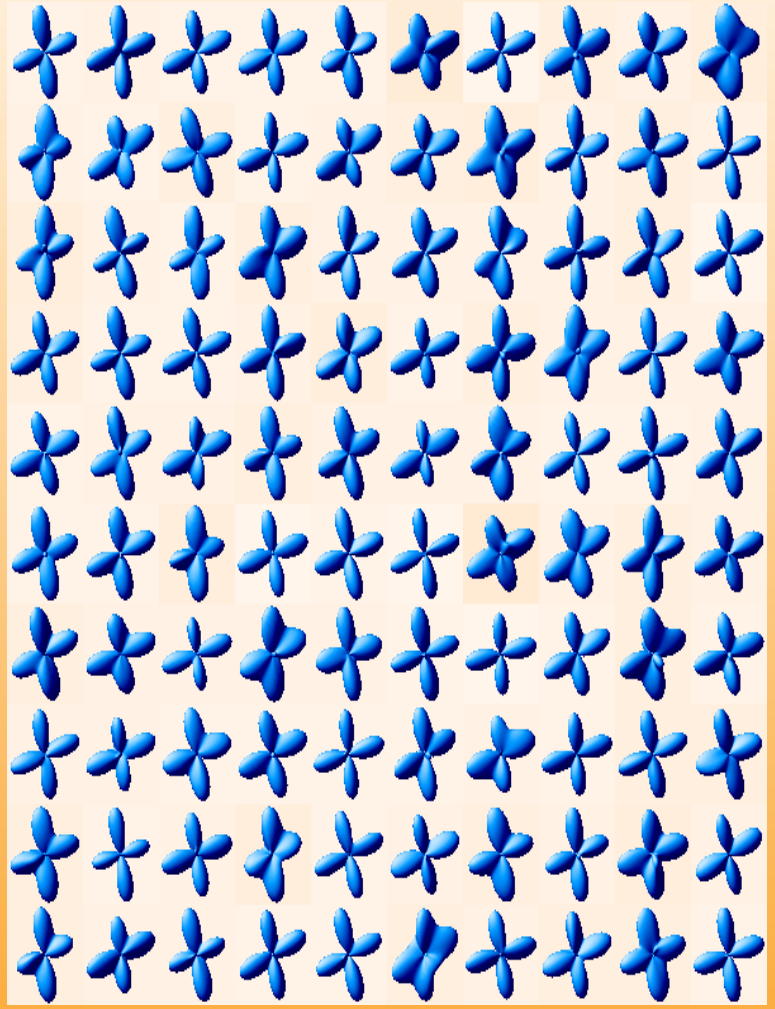

(b) Proposed method

Resistance to noise (3-fibers, $\sigma = 0.04$)

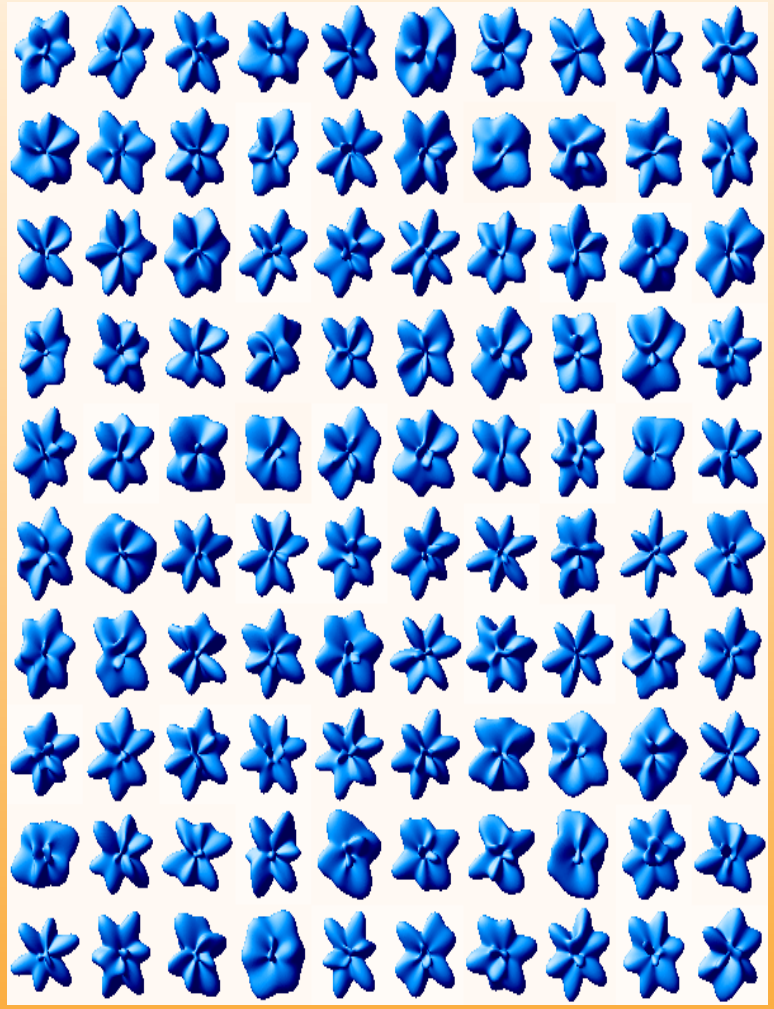

(a) ODF from QBI

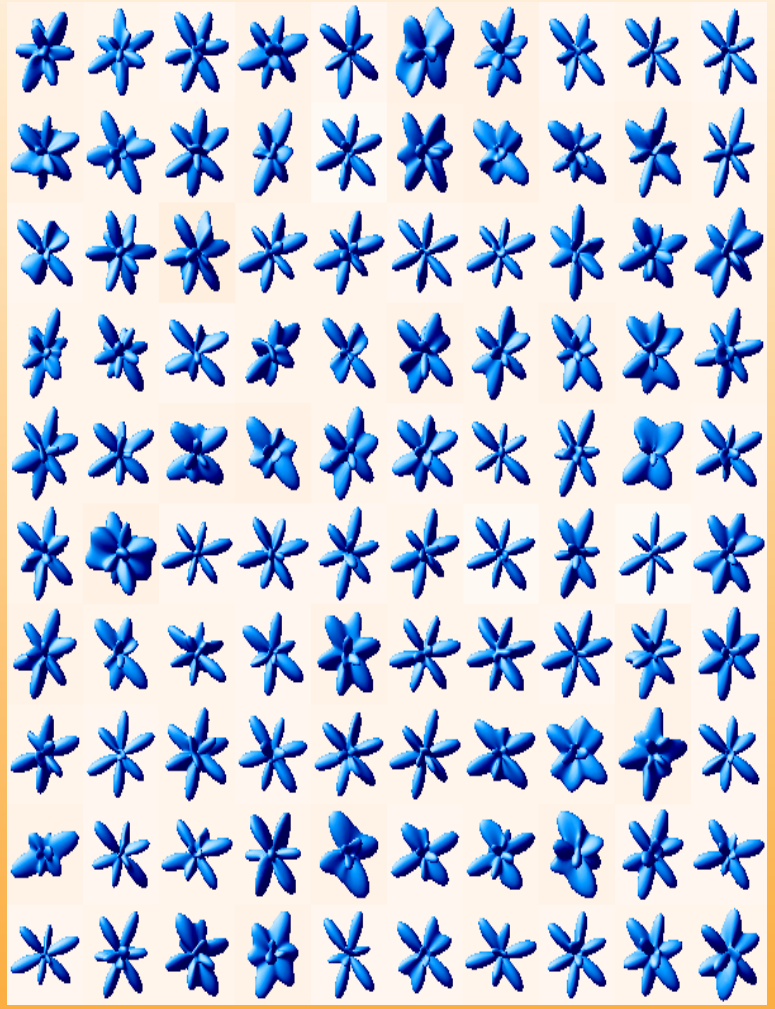

(b) Proposed method

Deviation angles

From proposed method

	$\psi(\sigma = 0)$	$\psi(\sigma = .02)$	$\psi(\sigma = .04)$	$\psi(\sigma = .06)$	$\psi(\sigma = .08)$
1 fiber	{ 0.243}	0.65 ± 0.39	1.19 ± 0.65	1.66 ± 0.87	2.19 ± 1.27
2 fibers	{0.74}	1.18 ± 0.66	2.55 ± 1.29	3.85 ± 2.12	4.91 ± 3.26
	{0.69}	1.30 ± 0.66	2.76 ± 1.34	3.63 ± 1.91	5.11 ± 2.65
3 fibers	{1.02}	4.87 ± 3.23	8.59 ± 5.82	11.79 ± 6.86	13.84 ± 8.73
	{0.97}	5.81 ± 3.61	7.70 ± 5.02	11.27 ± 6.36	12.54 ± 7.48
	{1.72}	4.92 ± 3.32	7.94 ± 4.59	12.57 ± 7.09	14.27 ± 7.66

From DOT

	$\psi(\sigma = 0)$	$\psi(\sigma = .02)$	$\psi(\sigma = .04)$	$\psi(\sigma = .06)$	$\psi(\sigma = .08)$
1 fiber	{0.414}	0.71 ± 0.35	1.08 ± 0.58	1.84 ± 0.88	2.20 ± 1.28
2 fibers	{1.55}	1.97 ± 0.96	3.37 ± 1.90	5.39 ± 2.99	7.00 ± 4.25
	{1.10}	1.73 ± 1.00	3.28 ± 1.87	4.78 ± 2.37	6.29 ± 3.19
3 fibers	{4.11}	7.89 ± 5.71	10.82 ± 6.66	14.56 ± 8.74	16.68 ± 10.21
	{3.46}	6.94 ± 3.70	11.28 ± 5.98	16.92 ± 10.36	17.02 ± 10.95
	{1.68}	6.76 ± 5.21	10.90 ± 5.63	14.08 ± 9.05	13.99 ± 9.74

From QBI

	$\psi(\sigma = 0)$	$\psi(\sigma = .02)$	$\psi(\sigma = .04)$	$\psi(\sigma = .06)$	$\psi(\sigma = .08)$
1 fiber	{0.089}	1.28 ± 0.75	3.34 ± 1.97	5.94 ± 3.19	7.67 ± 4.16
2 fibers	{0.45}	2.39 ± 1.26	4.82 ± 2.44	7.95 ± 4.45	8.91 ± 4.64
	{0.42}	2.30 ± 1.10	4.94 ± 2.15	7.49 ± 3.88	9.34 ± 4.45
3 fibers	{0.90}	10.80 ± 5.59	12.15 ± 4.42	20.21 ± 11.10	18.78 ± 11.39
	{0.90}	11.59 ± 5.44	13.07 ± 4.74	19.54 ± 11.80	20.79 ± 10.81
	{0.19}	11.66 ± 5.18	12.25 ± 4.93	20.36 ± 11.50	19.10 ± 10.18

Table: Mean and standard deviation values for the deviation angles ψ

Simulated data: two crossing fiber bundles

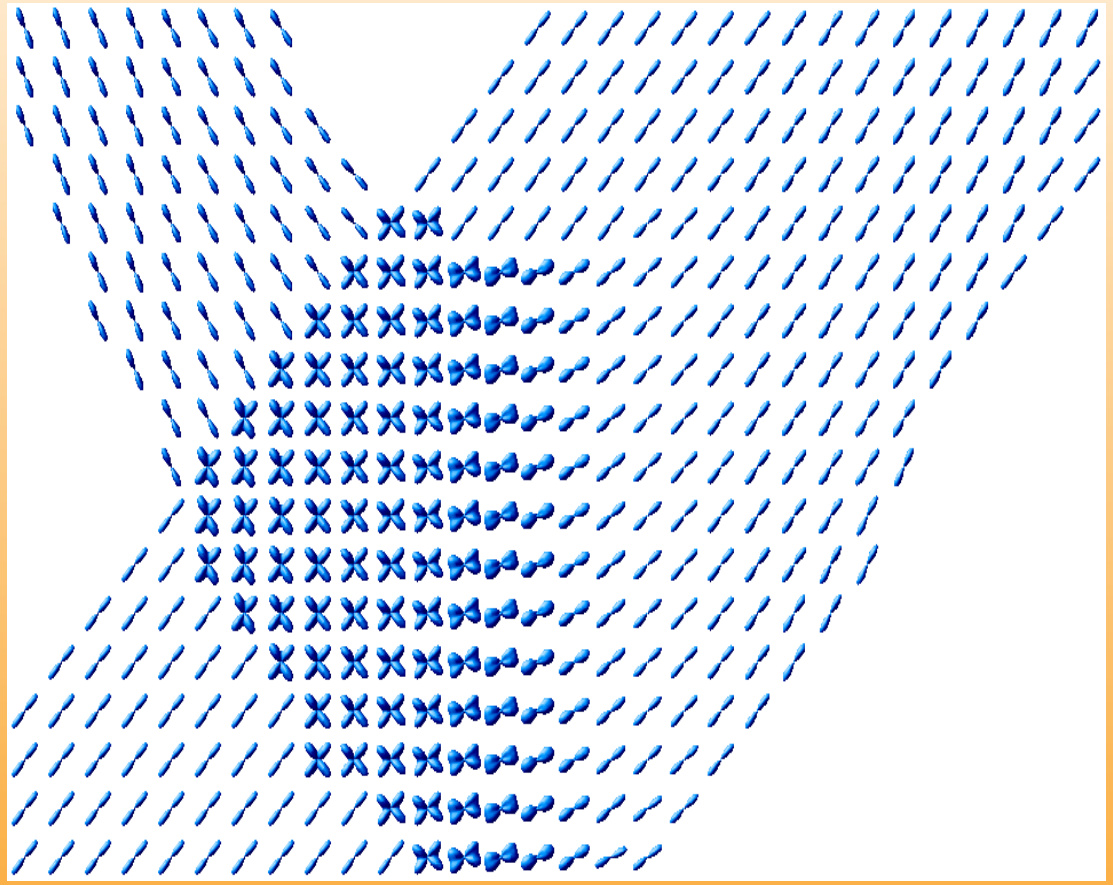

Figure: Probability maps from a simulated image of two crossing fiber bundles computed using proposed method

Real data: excised rat optic chiasm

Imaging parameters:

- Acquired at 14.1 T using Bruker Advance imaging systems.
- A diffusion-weighted spin echo pulse sequence was used
- Diffusion-weighted images were acquired along 46 directions with a b-value of $1250 s/mm^2$ along with a single image acquired at $b \approx 0 s/mm^2$
- Resolution: $33.6 \times 33.6 \times 200 \mu m^3$

Real data: excised rat optic chiasm

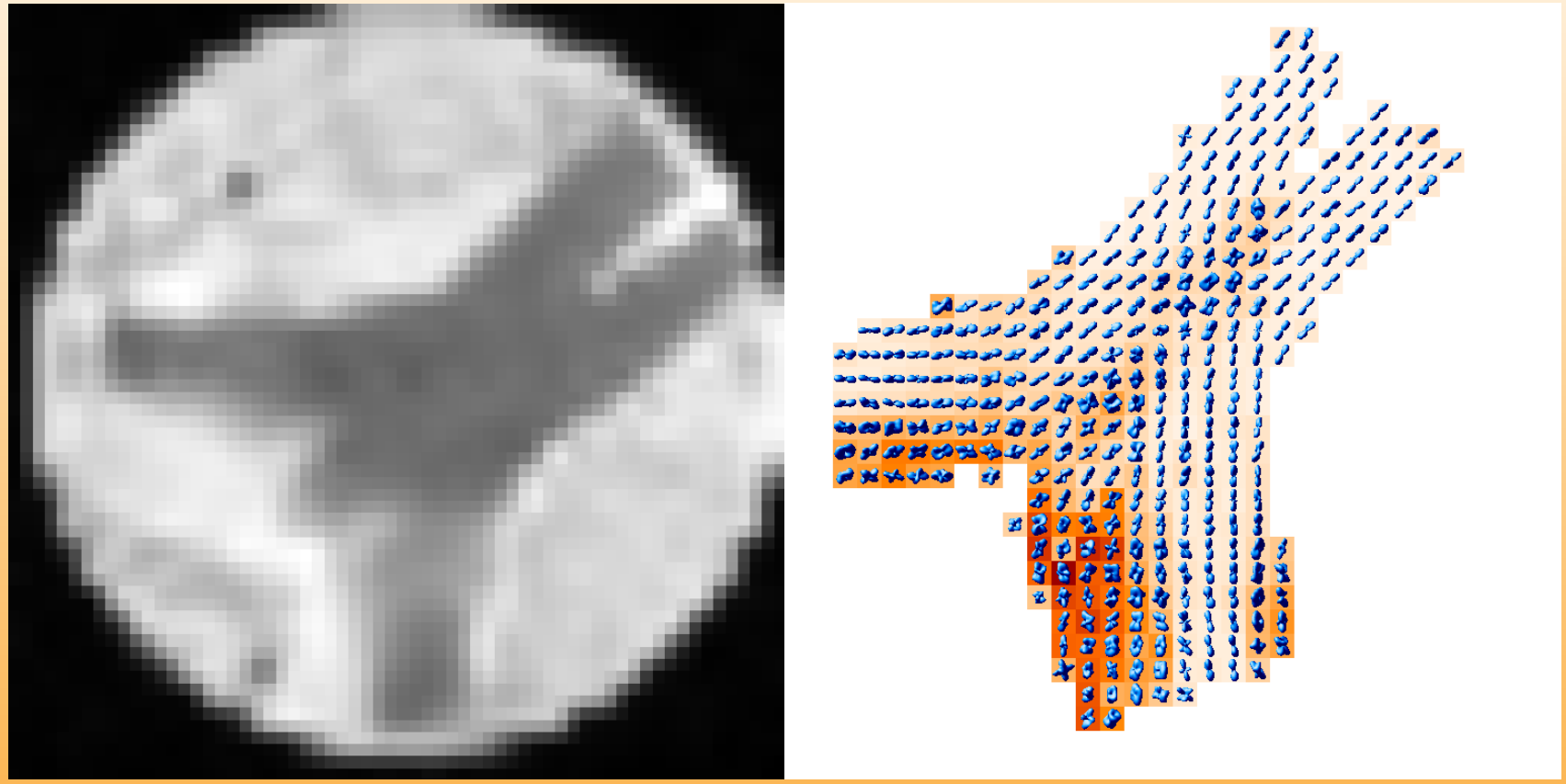

Figure: S0 image (Left) and probability maps (Right) computed from a rat optic chiasm data set overlaid on an axially oriented GA map

Real data: excised rat brain

Imaging parameters:

- Collected from an excised rat brain at 17.6T
- Consists of 52 images with varying orientations of the diffusion gradients.
  - 6 : with a $b \approx 125 s/mm^2$
  - 46: with $b \approx 1250 s/mm^2$
- Resolution: $75 \times 75 \times 300 \mu m^3$

S0 maps of control rat brain data

Figure: S0 map of a control rat brain. The rectangular region contains the hippocampus.

Probability surfaces from control rat brain data

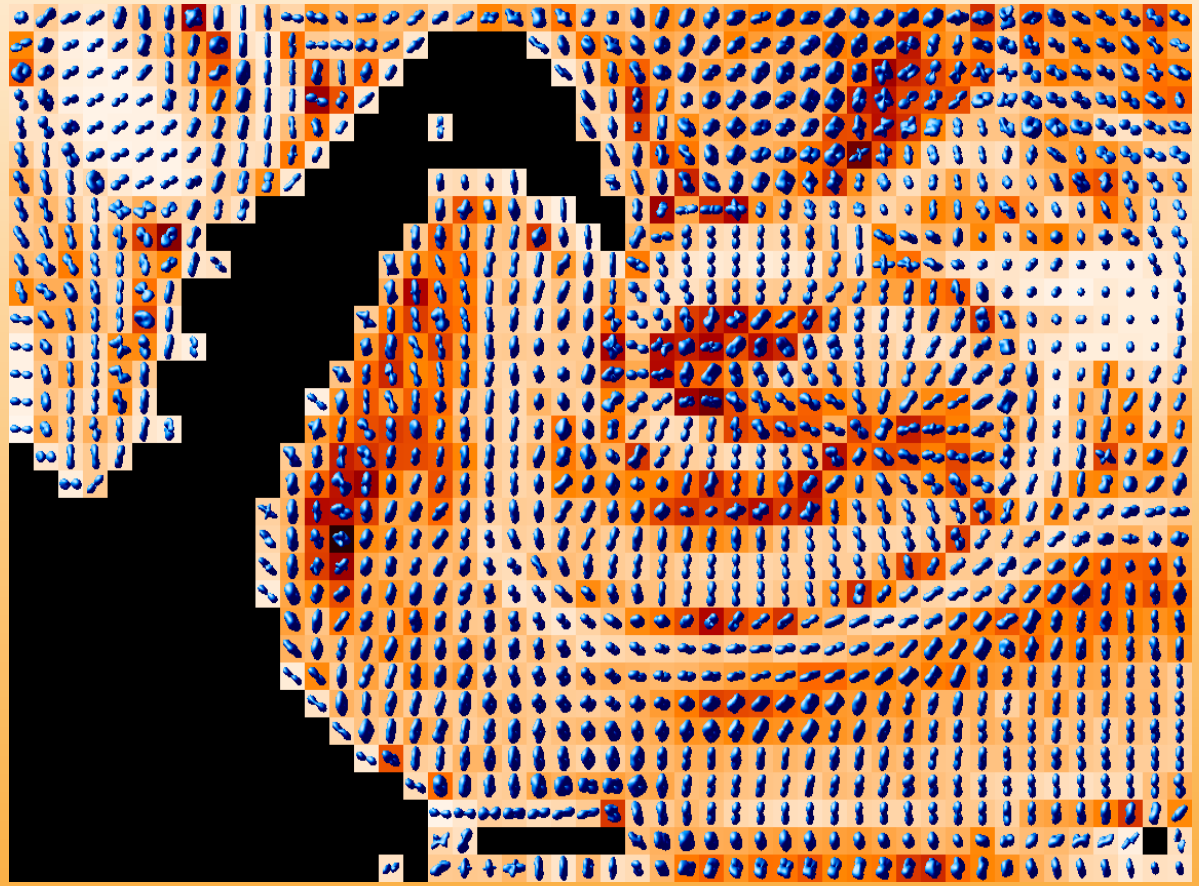

Figure: Probability surfaces computed from the hippocampus of a control rat brain

S0 map of epileptic rat brain data

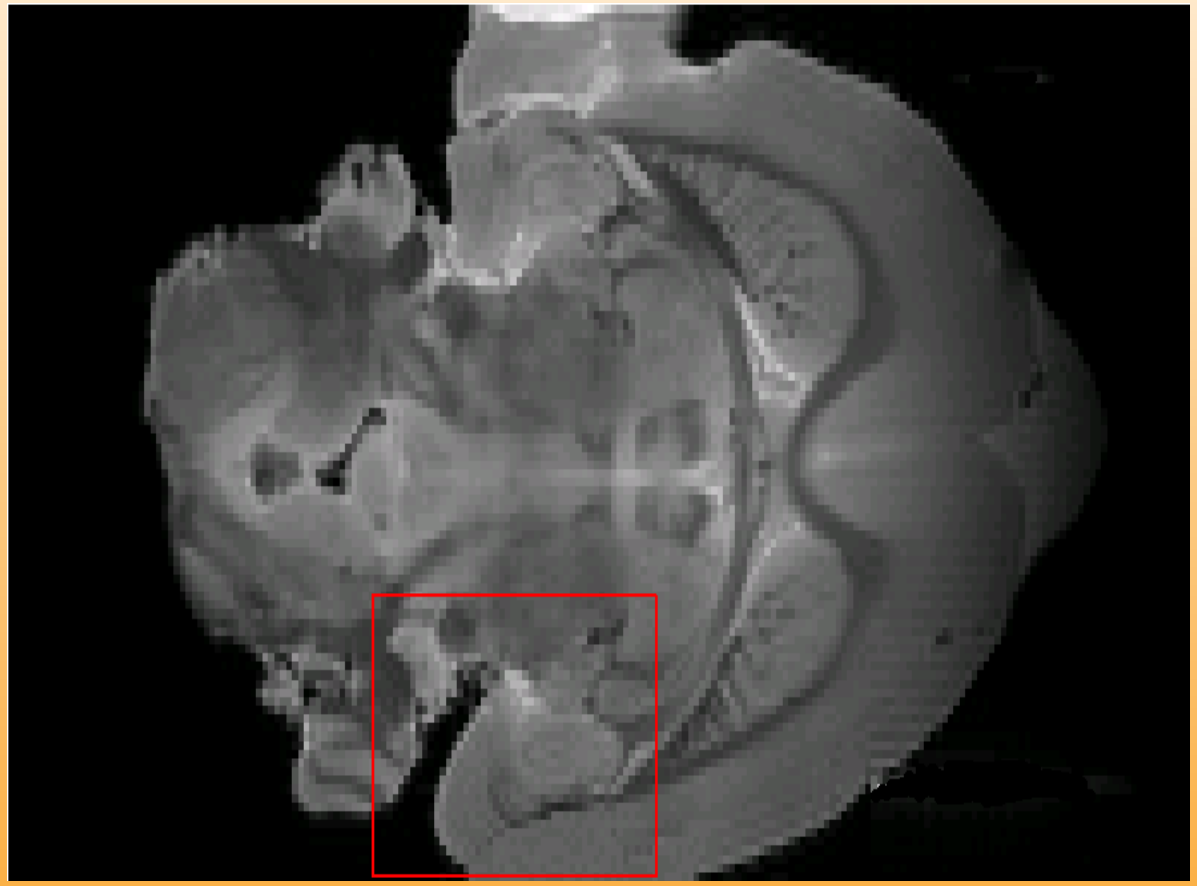

Figure: S0 map of an epileptic rat brain. The rectangular region contains the hippocampus.

Probability surfaces from epileptic rat brain data

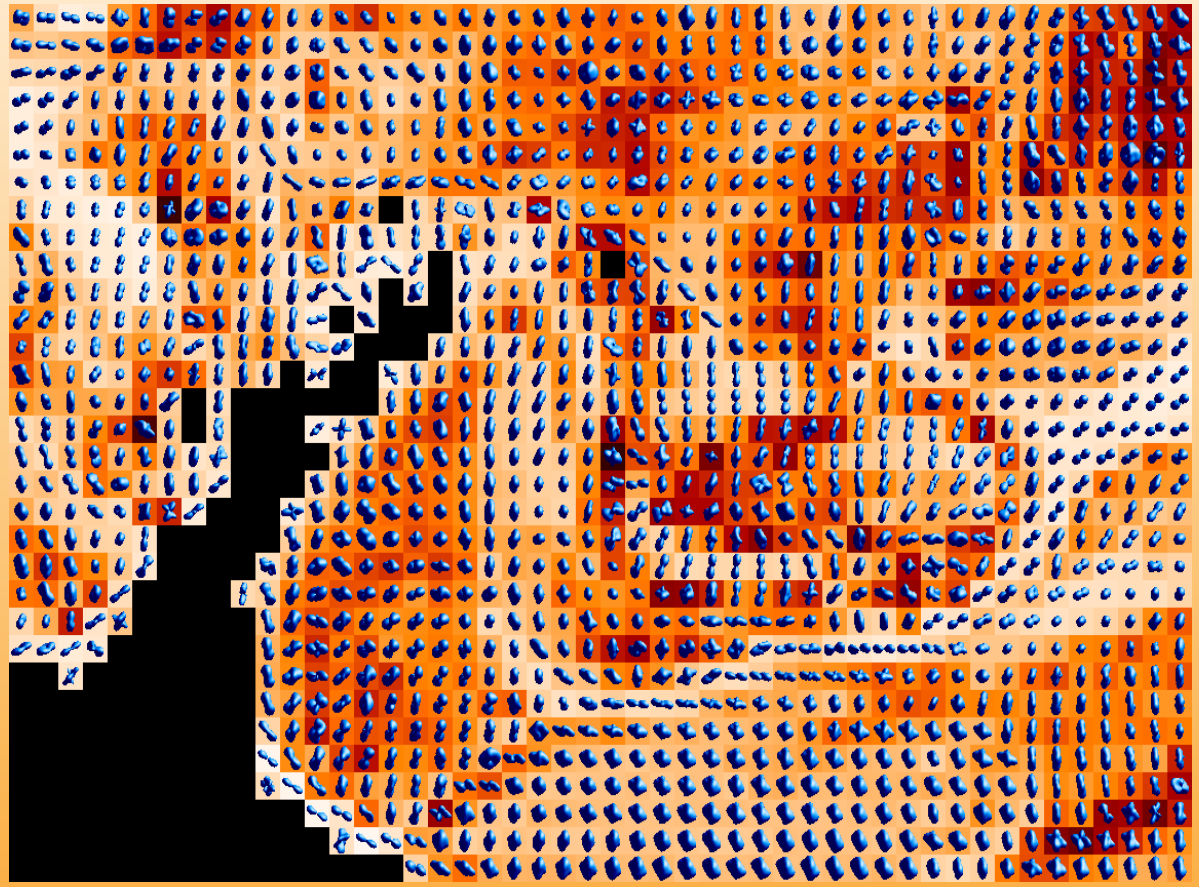

Figure: Probability surfaces computed from the hippocampus of an epileptic rat brain

Conclusions

- A novel continuous tensor distribution model was introduced.
- Signal was shown to be the Laplace transform of this distribution on $\mathcal{P}_n$
- For the Wishart and mixture of Wisharts, gave a closed form expression for this Laplace transform. DTI is a special case of this model.
- This lead to a novel Linear System for estimating the mixture of tensors from the signal measurements.

Conclusions

- A novel continuous tensor distribution model was introduced.
- Signal was shown to be the Laplace transform of this distribution on $\mathcal{P}_n$
- For the Wishart and mixture of Wisharts, gave a closed form expression for this Laplace transform. DTI is a special case of this model.
- This lead to a novel Linear System for estimating the mixture of tensors from the signal measurements.

Conclusions

- A novel continuous tensor distribution model was introduced.
- Signal was shown to be the Laplace transform of this distribution on $\mathcal{P}_n$
- For the Wishart and mixture of Wisharts, gave a closed form expression for this Laplace transform. DTI is a special case of this model.
- This lead to a novel Linear System for estimating the mixture of tensors from the signal measurements.

Conclusions

- A novel continuous tensor distribution model was introduced.
- Signal was shown to be the Laplace transform of this distribution on $\mathcal{P}_n$
- For the Wishart and mixture of Wisharts, gave a closed form expression for this Laplace transform. DTI is a special case of this model.
- This lead to a novel Linear System for estimating the mixture of tensors from the signal measurements.

Conclusions (Contd.)

- Showed expts. depicting better accuracy of reconstructed fiber orientations compared to Q-ball ODF and DOT for 1- 2- and 3- fibers in a voxel under varying noise.
- Advantage over discrete mixing model: No need to specify the number of components in the mixing density.
- Future work: Spatial regularization, fiber tracking (prior work: Campbell et al., Miccai'05), segmentation (prior work: McGraw et al., ECCV'06) etc.

Conclusions (Contd.)

- Showed expts. depicting better accuracy of reconstructed fiber orientations compared to Q-ball ODF and DOT for 1- 2- and 3- fibers in a voxel under varying noise.
- Advantage over discrete mixing model: No need to specify the number of components in the mixing density.
- Future work: Spatial regularization, fiber tracking (prior work: Campbell et al., Miccai'05), segmentation (prior work: McGraw et al., ECCV'06) etc.

Conclusions (Contd.)

- Showed expts. depicting better accuracy of reconstructed fiber orientations compared to Q-ball ODF and DOT for 1- 2- and 3- fibers in a voxel under varying noise.
- Advantage over discrete mixing model: No need to specify the number of components in the mixing density.
- Future work: Spatial regularization, fiber tracking (prior work: Campbell et al., Miccai'05), segmentation (prior work: McGraw et al., ECCV'06) etc.

Acknowledgements

- Funding from NIH NINDS RO1 NS42075 and RO1 EB007082.
- Thanks to collaborators: Bing Jian (PhD student), Evren Ozarslan (Postdoc at NIH, formerly at UF), Paul Carney MD (Neuroscience and Pediatrics), Thomas Mareci (Prof., BioChemistry and Molecular Biology).

Acknowledgements

- Funding from NIH NINDS RO1 NS42075 and RO1 EB007082.
- Thanks to collaborators: Bing Jian (PhD student), Evren Ozarslan (Postdoc at NIH, formerly at UF), Paul Carney MD (Neuroscience and Pediatrics), Thomas Mareci (Prof., BioChemistry and Molecular Biology).